Optics Letters

Mid-infrared frequency comb with 6.7 W average power based on difference frequency generation

Anthony Catanese,[1,†] Jay Rutledge,[1,†] Myles C. Silfies,[1] Xinlong Li,[1] Henry Timmers,[2,3] Abijith S. Kowligy,[2,3] Alex Lind,[2,3] Scott A. Diddams,[2,3] and Thomas K. Allison[1,*]

[1]Stony Brook University, Stony Brook, New York 11794, USA
[2]National Institute of Standards and Technology, Boulder, Colorado 80305, USA
[3]Department of Physics, University of Colorado Boulder, Boulder, Colorado 80309, USA
*Corresponding author: thomas.allison@stonybrook.edu

Received 11 December 2019; accepted 17 January 2020; posted 29 January 2020 (Doc. ID 385294); published 27 February 2020

We report on the development of a high-power mid-infrared frequency comb with 100 MHz repetition rate and 100 fs pulse duration. Difference frequency generation is realized between two branches derived from an Er:fiber comb, amplified separately in Yb:fiber and Er:fiber amplifiers. Average powers of 6.7 W and 14.9 W are generated in the 2.9 μm idler and 1.6 μm signal, respectively. With high average power, excellent beam quality, and passive carrier-envelope phase stabilization, this light source is a promising platform for generating broadband frequency combs in the far infrared, visible, and deep ultraviolet.

https://doi.org/10.1364/OL.385294

The extension of optical frequency comb techniques to the mid-infrared (mid-IR) has been mainly motivated by applications in molecular spectroscopy, including spectroscopy in the "fingerprint" region [1,2] and trace-gas sensing with high discrimination [3,4]. The development of mid-IR combs at the < 1 W level for molecular spectroscopy has thus been an area of intense activity. A variety of mid-IR frequency comb technologies have emerged over the last decade, among them mode-locked quantum cascade lasers [5], microresonator combs [6], and combs based on optical parametric amplifiers (OPA) [7] and optical parametric oscillators (OPO) [8].

In addition to spectroscopy, the mid-IR is also an excellent region for driving nonlinear optics. The 2–5 μm wavelength range is particularly attractive because it offers advantages for generating both coherent ultraviolet/visible light via high harmonic generation (HHG) [9–11], and broadband IR combs via difference frequency generation [12,13] or supercontinuum generation [14]. For HHG in gases, the mid-IR offers extension of the cutoff photon energy via scaling of the pondermotive energy [10]. For HHG in solids, the low mid-IR photon energy enables driving nonperturbative photocurrents [11] or cascaded $\chi^{(2)}$ and $\chi^{(3)}$ processes [9] without damage due to multiphoton absorption. For broadband IR continuum generation via intrapulse difference frequency generation (DFG), using driving wavelengths in the mid-IR enjoys much better group velocity matching compared to driving with more conventional near-IR combs, enabling high average powers and superoctave coherent IR bandwidths [12,13]. In these ways, the 2–5 μm spectral range offers a pivot to generating both shorter and longer wavelengths.

For driving nonlinear optics efficiently at high repetition rate, high average powers are needed. For this application, frequency combs based on DFG then offer several advantages. For power scaling, no heat (ideally) is deposited in parametric gain media, and with DFG combs based on multiple branches, the separate branches can be amplified to high average powers in fiber amplifiers [15–17]. For nonperturbative nonlinear optics sensitive to the electric field (e.g., solid-state HHG), OPAs based on DFG between a pump and signal derived from the same comb are particularly attractive due to passive elimination of the carrier-envelope offset frequency, f_0, producing a train of carrier-envelope phase (CEP) stable pulses. This stands in contrast to competing technologies based on Cr:ZnS [18] or Tm:fiber [19], for which it is nontrivial to stabilize f_0 to zero.

In this Letter, we present a 2.9 μm frequency comb based on high-power DFG in a two-stage OPA, operating at 100 MHz repetition rate with 6.7 W average power and 100 fs pulse duration. To our knowledge, this is the highest power mid-IR optical frequency comb reported to date and among the highest average power ultrafast mid-IR light sources in general. Furthermore, we demonstrate that this OPA can generate sufficient bandwidth to support few-cycle mid-IR pulses with further refinement of the seeding signal branch.

A schematic of our design is shown in Fig. 1. The pump (1035 nm) and signal (1500–1650 nm) are both derived from an all polarization-maintaining (PM) fiber Er:fiber oscillator (Menlo Systems M-comb ultralow noise variant) with a center wavelength of 1560 nm. In addition to convenient pulse synchronization, deriving both pump and signal combs from the same oscillator ensures the idler comb generated via DFG has $f_0 = 0$.

The pump branch uses an intricate yet robust chain of nonlinear fiber optics to shift the Er:fiber comb from 1560 nm

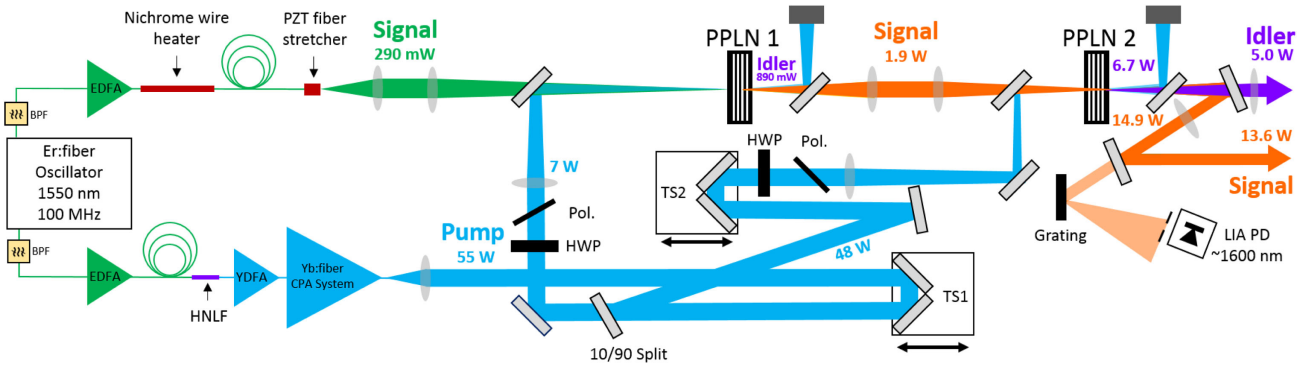

Fig. 1. Schematic of the two-stage OPA. Pump and signal branches are derived from an Er:fiber oscillator and are amplified in separate Er:fiber (EDFA) and Yb:fiber (YDFA) amplifiers. Difference frequency generation in two periodically poled lithium niobate crystals (PPLN1 and PPLN2) generates the high-power signal and idler combs. Path length stabilization is achieved by heating the fiber in the signal branch with a nichrome heater wire. Translation stage TS1 controls the pump/signal delay in both OPA stages, with TS2 changing only stage 2. More details in the text.

to 1035 nm [20]. From the Er:fiber oscillator, the light is bandpass-filtered (10 nm, BPF) and amplified in a nonlinear erbium-doped fiber amplifier (EDFA) incorporating normal-dispersion Er-doped fiber (1.5 m Er80-4/125-HD-PM, $D \approx -22$ ps/nm/km, 80 dB/m absorption at 1530 nm) pumped by four 750 mW, 976 nm pump diodes. After a length of anomalous dispersion fiber after the EDFA (30 cm, $D \approx 18$ ps/nm/km), sub-50 fs pulses with 350 mW average power enter a 3 cm long piece of anomalous dispersion ($D = 5.6$ ps/nm/km, $\gamma = 10.5\ \mathrm{W^{-1}\,km^{-1}}$, OFS Specialty Photonics) highly nonlinear fiber (HNLF) directly spliced to the anomalous dispersion fiber. Dispersive wave generation in the HNLF gives a comb with ~ 15 mW of power between 1000 and 1100 nm. All components of this fiber assembly are PM for excellent long-term stability. The output of the HNLF is subsequently amplified to 200 mW in a nonlinear, single-mode fiber, core-pumped, Yb-doped fiber amplifier (YDFA) and stretched to ~ 100 ps using an anomalous third-order dispersion fiber stretcher [21]. This light is then used to seed a two-stage high-power chirped-pulse YDFA system previously described in Ref. [21], giving up to 55 W and 180 fs pulses after grating-pair compression.

The signal branch is comparatively much simpler. A similar nonlinear EDFA is used, but with a longer 75 cm single-mode anomalous-dispersion fiber spliced to its output. This provides 290 mW and the complicated spectrum shown as the green curve of Fig. 2(C) for seeding the OPA. The total optical path length difference of ~ 20 m between the two branches, with high-power fiber amplifiers in both arms of the interferometer, is subject to long-term thermal drift. To stabilize the delay between the pump and signal at the OPA, the signal branch is equipped with two actuators. A piezoelectric fiber stretcher, driven with a 1071 Hz 20 V amplitude sine wave, modulates the signal seed delay by approximately 1 fs, which results in 0.1% amplitude modulation on the output of the OPA. This amplitude modulation is detected with a photodiode and a lock-in amplifier (LIA PD) to give an error signal. The error signal is integrated using a microcontroller, which controls heating current sent to 1 m of nichrome wire kapton taped directly to the EDFA gain fiber. A current of ~ 1 A increases the fiber temperature by approximately 30°C, and gives 1.1 ps of delay. With this setup, the path length can be stabilized indefinitely after an initial warm-up period.

The OPA itself is done in two stages using 5%-MgO-doped periodically poled lithium niobate (PPLN). A 2 mm long PPLN crystal, with a poling period of 30.49 μm, was ultimately chosen for both stages, but we report results with both 1 mm and 2 mm long crystals for PPLN2. The crystals are heated to 80°C to optimize phase matching and avoid photorefractive damage. Two stages offers several advantages for the high-power OPA. First, as discussed by Arisholm *et al.* [22], it is generally easier to achieve good beam quality in high-gain OPAs with multiple stages. Second, independent control of the pump/signal delay in each stage (via the translation stages shown in Fig. 1) allows partial

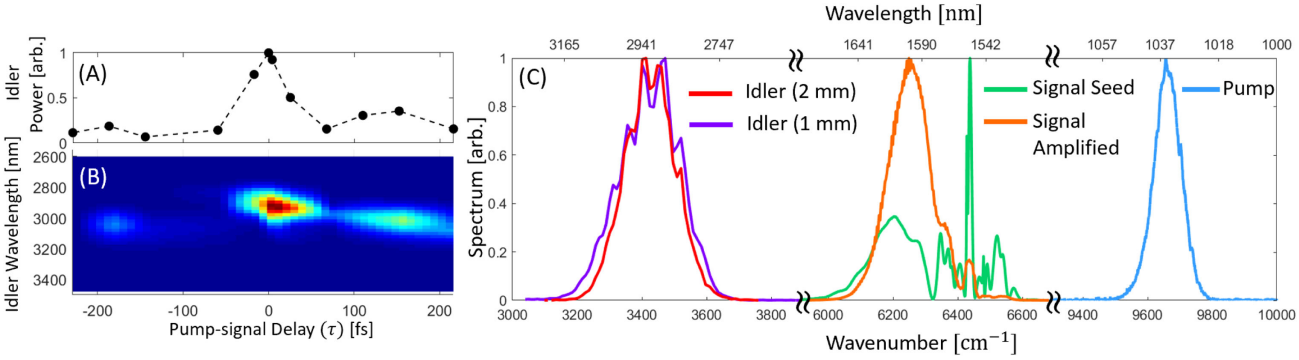

Fig. 2. Normalized stage 2 (A) idler power and (B) idler spectrum versus pump-signal delay τ. Positive τ indicates that the pump is arriving after the signal. (C) Spectrum of the pump, signal seed, signal output, and idler output of the OPA at $\tau = 0$. The two idler spectra shown are for 1 and 2 mm PPLN crystals in stage 2.

compensation of the pump/signal group velocity walk-off in stage 1. The pump power of each OPA stage is independently adjustable using a combination of a half-wave plate (HWP) and thin film polarizer (Pol.). With 55 W from the YDFA, up to 7 W and 48 W can be used to pump stages 1 and 2, respectively. The pump light is focused to spot sizes of 78 μm and 161 μm (FWHM) in stage 1 and 2, respectively. The signal beam in each stage is focused to the same size as the pump. We have not observed crystal damage over several months of operation.

Figures 2(A) and 2(B) show the OPA output power and idler spectrum as the pump/signal delay, τ, for both OPA stages is varied using translation stage TS1, showing multiple pulses emerging from the anomalous dispersion fiber. $\tau = 0$ is taken to be the delay of highest idler power. Mid-IR spectra were acquired using a scanning 1/3-m Czerny–Turner monochromator and liquid-nitrogen cooled InSb photodetector. The highest output power is observed when the OPA output spectrum is centered at 2900 nm, with the corresponding amplified signal spectrum [orange curve of Fig. 2(C)] centered at 1600 nm. This well-isolated pulse at $\tau = 0$, trailing the main 1550 nm pulse at $\tau = -200$ fs, corresponds to a Raman-shifted soliton generated in the long anomalous dispersion fiber pigtail of the signal-branch EDFA. Thus, despite the complicated temporal structure emerging from the simple signal branch fiber assembly, clean soliton pulses can be isolated for amplification in the OPA. For the rest of the paper, we present results recorded at $\tau = 0$.

When pumping the first stage with 7 W, more than 2 W of signal light and 900 mW of idler light emerge from PPLN1. Only the signal is retained between stage 1 and stage 2. With 48 W pump power in stage 2, at the exit of PPLN2 there are 6.7 W of idler and 14.9 W of signal. Figure 3(A) shows the idler output power versus stage 2 pump power. Curves are shown for both 1 mm and 2 mm long PPLN crystals. The idler is isolated from the signal and pump via two dichroic mirrors and collimated with an $f = 25$ cm CaF_2 lens. The dashed lines are the measured power after these output optics and represent the usable idler power from the OPA, while the solid curves represent the output power corrected for the measured 25% losses in the output optics. With the current output optics, the

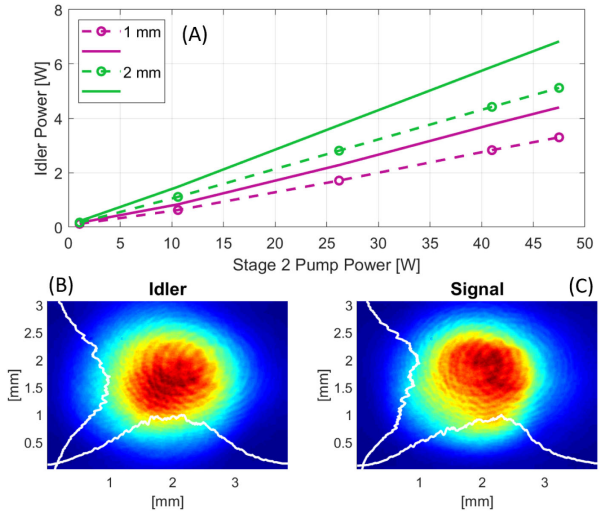

Fig. 3. (A) Stage 2 idler power versus pump power for both 1 mm and 2 mm long crystals. Dashed lines indicate the measured power after separating and collimating optics. Spatial mode profiles of (B) the idler and (C) the signal at full power. Vertical and horizontal profiles along lineouts intersecting the centroid are shown in white.

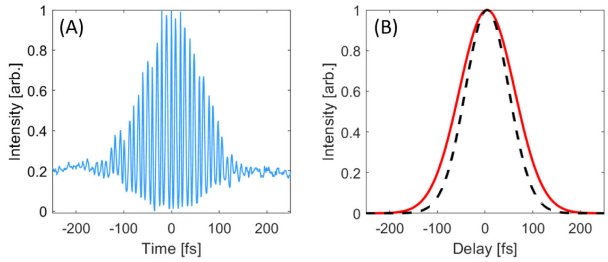

Fig. 4. (A) Idler interferometric autocorrelation for the PPLN2 = 2 mm thick crystal. (B) Intensity autocorrelation from low-pass filtering (red), which assuming a Gaussian pulse shape, corresponds to a measured idler pulse duration of 96 fs. Calculated autocorrelation (black) for a transform-limited pulse with the spectrum shown in Fig. 2(C).

2 mm (1 mm) long PPLN yields 5 W (3.3 W) usable idler power after the dichroic mirrors. Figure 3(B) also shows the output spot profiles at full power, measured using an additional 0.5x telescope and a microbolometer array camera. Despite the high powers involved, excellent beam quality is observed in both the signal and idler spatial modes.

Figure 4(A) shows an interferometric autocorrelation of the idler pulse, measured using a Michelson interferometer with a two-photon InGaAs photodiode detector. Figure 4(B) shows the intensity autocorrelation obtained from low-pass filtering the data. Assuming a Gaussian pulse shape, the measured idler pulse duration is determined to be 96 fs (FHWM). The transform-limited pulse calculated from the idler spectrum of Fig. 2(C) has a FWHM of 78 fs. For comparison with the experimental data, we also calculated the autocorrelation that the transform-limited idler pulses would have produced, and this is shown in dashed black.

Figure 5 shows the relative intensity noise (RIN) in units of dBc/Hz for the idler output, signal output, pump, and signal seed, acquired with a multichannel 16-bit digitizer with analog antialiasing filters (Picoscope 4262). Analysis of the corresponding time series data indicated that idler and signal noise are strongly correlated, but uncorrelated from the noise of the pump and signal seed. Interestingly, we observed the RIN levels to not depend strongly on the pump/signal delay, in contrast to other recent reports [23,24].

Finally, we address the current OPA bandwidth and what is attainable with this platform. Figure 2(C) shows the idler spectrum for either the 1 and 2 mm PPLN crystals in the second OPA stage. The bandwidth obtained is nearly the same.

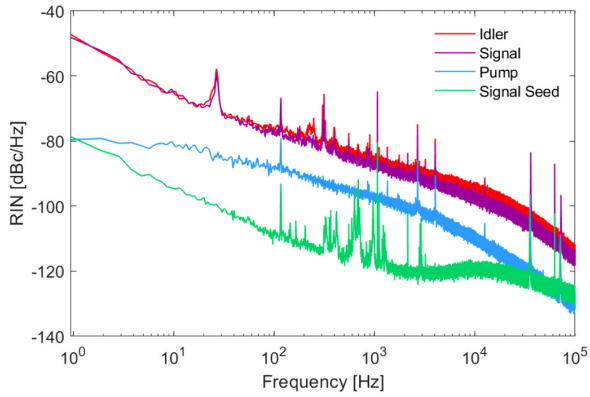

Fig. 5. RIN for idler, signal output, pump, and signal seed.

Similarly, the pulse duration measured with 1 and 2 mm crystals is also the same within experimental error. This indicates that the bandwidth and pulse duration are not limited by the group velocity walk-off in PPLN2, but instead by the fragmented signal seed pulse. Further evidence that the OPA can support much larger bandwidths is seen in Fig. 2(B), where output idler spectra are recorded as the pump/signal delay is varied. Parametric gain is achieved over ~ 400 nm ($450\ \mathrm{cm}^{-1}$) of bandwidth with a single poling period and crystal temperature. To further explore this, we modeled the OPA in one spatial dimension as a $\chi^{(2)}$ three-wave mixing of temporally Gaussian pulses according to [16]. We applied the Fourier split-step method to solve two sequentially and independently pumped stages of PPLN, with 25 fs transform-limited input seed pulses and 2 mm PPLN crystals in both stages. The results of the simulation predict that > 400 nm phase-matched bandwidths supporting transform-limited pulses of less than 35 fs duration, or less than 3.5 optical cycles, can be attained.

In this Letter, we have presented the design and performance of a high-power mid-IR frequency comb based on DFG. The system has demonstrated the ability to produce 6.7 W of 2.9 μm idler light and 14.9 W of 1.6 μm signal light with excellent beam quality and measured idler pulse duration of 100 fs. We have also shown that the OPA is capable of supporting larger bandwidths and shorter, even few-cycle pulses, with further refinement of the seed branch. Very short 1550 nm pulses for seeding the OPA can be generated using a similar nonlinear EDFA seed branch by using short normal dispersion HNLFs, as in Ref. [2], and we plan to implement this in the future. With few-cycle pulses and intrinsic CEP stability, this source is attractive for driving nonperturbative HHG in solids, with the possibility of generating isolated attosecond vacuum ultraviolet pulses at high repetition rate via gating schemes [11]. The high-power signal beam offers additional opportunities. Even with the current usable idler parameters of 5 W of average power and 100 fs pulse duration, focusing to 6 μm (2λ) FWHM would yield peak intensities of $1.6 \times 10^{12}\ \mathrm{W/cm}^2$, sufficient to reach the nonperturbative HHG regime in a variety of crystals [11]. We note that solid-state HHG at ~ 100 MHz rate has recently been achieved using alternative high-power, but not CEP-stable, mid-IR sources [18,19]. Finally, using this high-power DFG comb, we have recently realized cascaded HHG in PPLN waveguides at 100 MHz for the generation of broadband visible frequency combs [25], and in this work we have also verified the coherence of the idler comb via heterodyne characterization of its high harmonics. This OPA platform can also be used for tunable high-power mid-IR comb generation if dispersive wave generation is implemented in the signal branch and the PPLN poling period tuned as in Ref. [16].

Funding. National Science Foundation (1708743); Air Force Office of Scientific Research (FA9550-16-1-0016, FA9550-16-1-0164); U.S. Department of Education (GAANN); Defense Advanced Research Projects Agency (SCOUT).

Acknowledgment. M.C. Silfies and A. Catanese acknowledge support from the GAANN program of the U.S. Dept. of Education. The mention of specific products or trade names does not constitute an endorsement by NIST.

Disclosures. The authors declare no conflicts of interest.

[†]These authors contributed equally to this work.

REFERENCES

1. P. B. Changala, M. L. Weichman, K. F. Lee, M. E. Fermann, and J. Ye, Science **363**, 49 (2019).
2. H. Timmers, A. Kowligy, A. Lind, F. C. Cruz, N. Nader, M. Silfies, G. Ycas, T. K. Allison, P. G. Schunemann, S. B. Papp, and S. A. Diddams, Optica **5**, 727 (2018).
3. A. Foltynowicz, P. Masłowski, A. J. Fleisher, B. J. Bjork, and J. Ye, Appl. Phys. B **110**, 163 (2013).
4. L. Nugent-Glandorf, F. R. Giorgetta, and S. A. Diddams, Appl. Phys. B **119**, 327 (2015).
5. A. Hugi, G. Villares, S. Blaser, H. C. Liu, and J. Faist, Nature **492**, 229 (2012).
6. K. Luke, Y. Okawachi, M. R. E. Lamont, A. L. Gaeta, and M. Lipson, Opt. Lett. **40**, 4823 (2015).
7. A. Ruehl, A. Gambetta, I. Hartl, M. E. Fermann, K. S. E. Eikema, and M. Marangoni, Opt. Lett. **37**, 2232 (2012).
8. F. Adler, K. C. Cossel, M. J. Thorpe, I. Hartl, M. E. Fermann, and J. Ye, Opt. Lett. **34**, 1330 (2009).
9. D. D. Hickstein, D. R. Carlson, A. Kowligy, M. Kirchner, S. R. Domingue, N. Nader, H. Timmers, A. Lind, G. G. Ycas, M. M. Murnane, H. C. Kapteyn, S. B. Papp, and S. A. Diddams, Optica **4**, 1538 (2017).
10. T. Popmintchev, M.-C. Chen, D. Popmintchev, P. Arpin, S. Brown, S. Ališauskas, G. Andriukaitis, T. Balčiunas, O. D. Mücke, A. Pugzlys, A. Baltuška, B. Shim, S. E. Schrauth, A. Gaeta, C. Hernández-Garca, L. Plaja, A. Becker, A. Jaron-Becker, M. M. Murnane, and H. C. Kapteyn, Science **336**, 1287 (2012).
11. S. Ghimire and D. A. Reis, Nat. Phys. **15**, 10 (2019).
12. S. Vasilyev, I. S. Moskalev, V. O. Smolski, J. M. Peppers, M. Mirov, A. V. Muraviev, K. Zawilski, P. G. Schunemann, S. B. Mirov, K. L. Vodopyanov, and V. P. Gapontsev, Optica **6**, 111 (2019).
13. C. Gaida, M. Gebhardt, T. Heuermann, F. Stutzki, C. Jauregui, J. Antonio-Lopez, A. Schülzgen, R. Amezcua-Correa, A. Tünnermann, I. Pupeza, and J. Limpert, Light Sci. Appl. **7**, 94 (2018).
14. M. Seidel, X. Xiao, S. A. Hussain, G. Arisholm, A. Hartung, K. T. Zawilski, P. G. Schunemann, F. Habel, M. Trubetskov, V. Pervak, O. Pronin, and F. Krausz, Sci. Adv. **4**, eaaq1526 (2018).
15. F. C. Cruz, D. L. Maser, T. Johnson, G. Ycas, A. Klose, F. R. Giorgetta, I. Coddington, and S. A. Diddams, Opt. Express **23**, 26814 (2015).
16. D. L. Maser, G. Ycas, W. I. Depetri, F. C. Cruz, and S. A. Diddams, Appl. Phys. B **123**, 142 (2017).
17. F. Zhu, H. Hundertmark, A. A. Kolomenskii, J. Strohaber, R. Holzwarth, and H. A. Schuessler, Opt. Lett. **38**, 2360 (2013).
18. G. Vampa, S. Vasilyev, H. Liu, M. Mirov, P. H. Bucksbaum, and D. A. Reis, Opt. Lett. **44**, 259 (2019).
19. K. F. Lee, X. Ding, T. J. Hammond, M. E. Fermann, G. Vampa, and P. B. Corkum, Opt. Lett. **42**, 1113 (2017).
20. G. Ycas, S. Osterman, and S. A. Diddams, Opt. Lett. **37**, 2199 (2012).
21. X. Li, M. A. R. Reber, C. Corder, Y. Chen, P. Zhao, and T. K. Allison, Rev. Sci. Instr. **87**, 093114 (2016).
22. G. Arisholm, R. Paschotta, and T. Südmeyer, J. Opt. Soc. Am. B **21**, 578 (2004).
23. V. S. de Oliveira, A. Ruehl, P. Maslowski, and I. Hartl, "Intensity noise optimization of a mid-infrared frequency comb difference frequency generation source," arXiv:1904.02611 (2019).
24. K. Krzempek, D. Tomaszewska, A. Głuszek, T. Martynkien, P. Mergo, J. Sotor, A. Foltynowicz, and G. Soboń, Opt. Express **27**, 37435 (2019).
25. A. Kowligy, J. Rutledge, A. Catanese, M. C. Silfies, S. A. Diddams, and T. K. Allison, are preparing a manuscript to be called "Efficient wideband UV/visible frequency comb generation via cascaded high-harmonic generation in lithium niobate waveguides."